Available online at www.sciencedirect.com
SCIENCE DIRECT®
Bioorganic & Medicinal Chemistry 12 (2004) 3797–3806
Bioorganic & Medicinal Chemistry

Probing the ultra-high resolution structure of aldose reductase with molecular modelling and noncovalent mass spectrometry

Connie Darmanin,[a] Guillaume Chevreux,[b] Noelle Potier,[b] Alain Van Dorsselaer,[b] Isabelle Hazemann,[c] Alberto Podjarny[c] and Ossama El-Kabbani[a,*]

[a]*Department of Medicinal Chemistry, Victorian College of Pharmacy, Monash University, Parkville, Vic. 3052, Australia*
[b]*Laboratoire de Spectrometrie de Masse Bio-Organique, CNRS UMR 7509, Strasbourg, France*
[c]*UPR de Biologie Structurale, IGBMC, CNRS INSERM ULP, Illkirch, France*

Received 27 December 2003; revised 9 May 2004; accepted 10 May 2004
Available online 8 June 2004

Abstract—Aldose reductase, the first and rate-limiting enzyme of the polyol pathway, is a target for drug design for the treatment of diabetes complications. The structures of aldose reductase in complex with the cyclic imide inhibitors Fidarestat and Minalrestat were recently determined at ultra-high resolution (*Proteins* **2004**, *55*, 805). We have used the detailed structural information revealed at atomic resolution, including the assignment of protonation states for the inhibitors and active site residues, together with molecular modelling and noncovalent mass spectrometry to characterise the type and strength of the interactions between the enzyme and the inhibitors, and to attempt the design of novel potential inhibitors with enhanced binding energies of the complexes. The VC_{50} values measured by mass spectrometry (accelerated voltage of ions needed to dissociate 50% of a noncovalent complex in the gas phase) for the aldose reductase inhibitors correlate with the IC_{50} values (concentration of inhibitor giving 50% inhibition in solution) and with the electrostatic binding energies calculated between the active site residues Tyr48, His110 and Trp111 and the inhibitors, suggesting that electrostatic interactions play a major role in inhibitor binding. Our molecular modelling and design studies suggest that the replacement of the fluorine atom in Minalrestat's bromo-fluorobenzyl group with nitro, amide and carboxylate functional groups enhanced the predicted net binding energies of the complexes by 16%, 31% and 68%, respectively. When the carbamoyl group of Fidarestat was replaced with a nitro, 4-hydroxyl phenyl and carboxylate functional groups, the predicted net binding energies of the complexes were enhanced by 13%, 34% and 46%, respectively.

1. Introduction

Aldose reductase (ALR2; EC 1.1.1.21), the first enzyme of the polyol pathway that converts glucose to sorbitol using NADPH as cofactor, is implicated in the development of diabetic complications such as glaucoma, neuropathies, nephropathies, retinopathies and cataracts.[1,2] During diabetic hyperglycaemia the increased flux of glucose through the polyol pathway results in biochemical imbalances in target tissues such as nerves, lens, retina and kidneys,[3,4] and as such inhibition of ALR2 represents an attractive strategy for the prevention of the complications.[4,5] ALR2 is homologous (65% identity) to aldehyde reductase (ALR1), an enzyme, which catalyses the NADPH-dependent reduction of diverse aldehydes to their corresponding alcohols.[6,7] Both enzymes belong to the aldo–keto reductase superfamily and the close similarities in their sequences and 3-D structures make it difficult to develop inhibitors specific only to ALR2. A superposition of the active site residues of ALR2 and ALR1 is shown in Figure 1. The least conserved residues in the two enzymes are located in the C-terminal loop, which lines a hydrophobic region of the active site called the 'specificity' pocket.[8,9]

The two main classes (Scheme 1) of ARL2 inhibitors (ARIs) are carboxylic acids (e.g., Statil) and cyclic imides (e.g., Sorbinil, Fidarestat and Minalrestat).[10–14] While both classes of inhibitors display similar potencies against ALR2 in vitro, cyclic imides are usually more potent in vivo, likely due to the difference in the pK_a values between the two classes. Carboxylic acids have low pK_a values (generally below 4), which makes them ionised at physiological pH and more difficult to cross

Keywords: Mass spectrometry; Molecular modelling; Aldose reductase; Ultra-high resolution; Drug design; Enzyme inhibitors.
* Corresponding author. Tel.: +61-3-9903-9691; fax: +61-3-9903-9582; e-mail: ossama.el-kabbani@vcp.monash.edu.au

0968-0896/$ - see front matter © 2004 Elsevier Ltd. All rights reserved.
doi:10.1016/j.bmc.2004.05.014

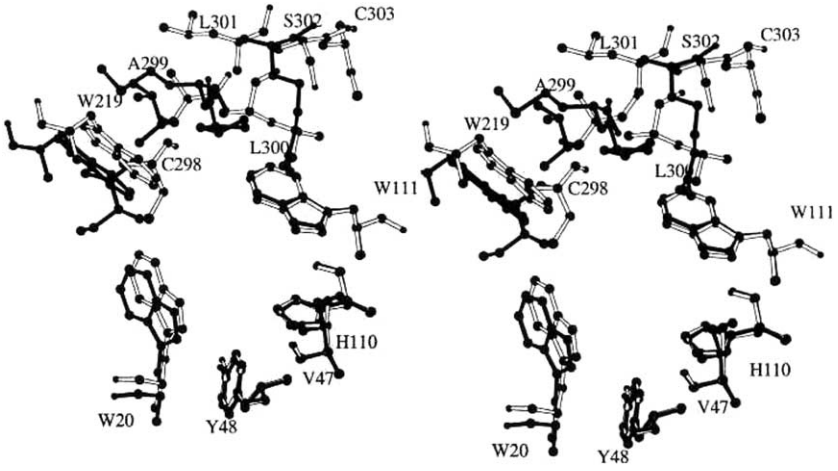

Figure 1. Superposition of the active site residues of ALR2 (white) and ALR1 (black) shown in stereo. The ALR2 residues are labelled with residue type and number.

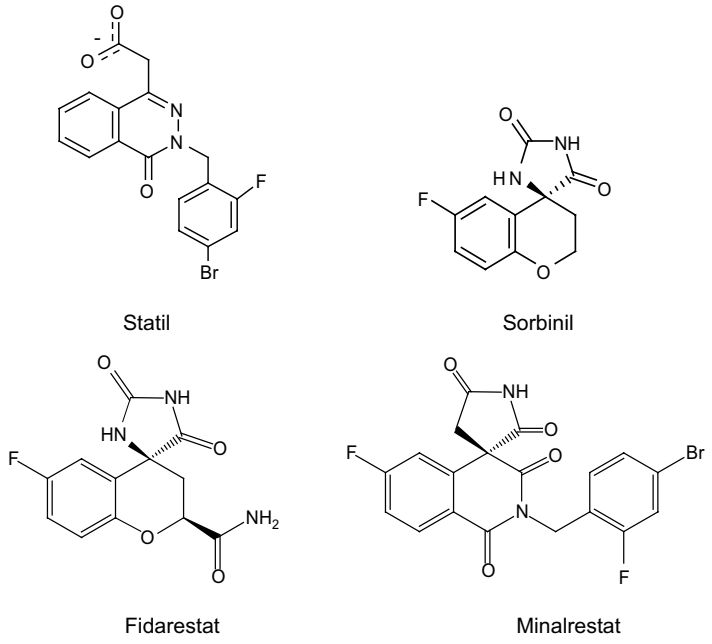

Scheme 1.

the biological membrane than cyclic imides, which have higher pK_a values (between 8 and 9).[15] Based on the atomic resolution structures of ALR2 in complex with Fidarestat and Minalrestat (PDB entry codes 1PWM and 1PWL) it has been suggested that cyclic imide inhibitors initially cross the biological membrane as neutral compounds, then lose a proton and bind to the active site of the enzyme with their negative charge contributing to the tight inhibitor binding.[16] This observation is supported by the fact that the translation from in vitro to in vivo activity for this class of compounds was usually easily achieved.[15]

The overall structure of human ALR2 folds into an eight-stranded α/β-barrel with the active site located at the C-terminal end of the barrel.[8,10] The $NADP^+$ binding site is located adjacent to a hydrophobic active site pocket. Fidarestat and Minalrestat are bound to the active site with their cyclic imide moiety entering the anion-binding site. This moiety is anchored in the active site and held in place by 13 van der Waals interactions with the nicotinamide ring of $NADP^+$.[16] Both carbonyl oxygen atoms are present within hydrogen bonding distances from the side chains of Trp111 and Tyr48, while His110 forms a hydrogen bond with the negatively charged 1′-position nitrogen atom in the cyclic imide substituent. The chroman ring of Fidarestat was located within van der Waals contacts with the side chains of residues Trp20, Trp111, Phe122 and Trp219. The carbonyl oxygen of the carbamoyl group was hydrogen bonded to the main-chain nitrogen atom of Leu300, which lines part of the 'specificity' pocket. This interaction was suggested to be responsible for the high affinity and selectivity of Fidarestat for ALR2 over

ALR1.[17] Minalrestat binds to ALR2 with its isoquinoline ring system located in a hydrophobic pocket formed mainly by the side chains of Trp20, Phe122 and Trp219. The 4-bromo-2-fluorobenzyl group enters the crevice formed between Phe122, Leu300 and Trp111. The benzyl group π-stacks against the side chain of Trp111, while the bromine atom is positioned within interacting distance with the side chain of Thr113 and the fluorine atom interacts with the main-chain amide of Leu300. The binding of Minalrestat is accompanied by a conformational change to the side chains of Leu300 and Phe122 that opens the 'specificity' pocket lined by residues Trp111, Thr113, Phe122, Ala299 and Leu300,[16] an observation supported by the temperature factor values, which tend to be 2–3-fold higher for the flexible residues lining the ALR2 active site compared to the other neighbouring residues. The RMS deviation between the active site residues complexed with Fidarestat and those complexed with Minalrestat is equal to 1.028 Å.

The interactions between inhibitors and ALR2 can be characterised using mass spectrometric analysis by measuring the gas-phase stability of the enzyme–inhibitor complexes.[18,19] Figure 2 illustrates the enzyme–inhibitor interaction. The VC_{50} values, unlike the IC_{50}, mostly reflect the enzyme–inhibitor electrostatic and hydrogen bonding interactions (Tyr48 OH, His110 Nε2, Trp111 NE1 and Thr113 OH), and exclude hydrophobic interactions (Phe122 and Trp111 side-chain rings).[20] We have complemented the 3-D structural information obtained at 0.92 Å resolution[16] (including the protonation states for the inhibitors and active site residues, and accurate determination of bond lengths of the inhibitors, coenzyme $NADP^+$ and amino acids) by mass spectrometry and molecular modelling studies to evaluate the type and strength of the enzyme–inhibitor interaction. Moreover, in an attempt to develop potent and more specific inhibitors of the enzyme, compounds that may capture the maximum interaction with the non-conserved C-terminal residues and may lead to enhanced binding energies were designed based on the atomic resolution models of the ALR2 ternary complexes.

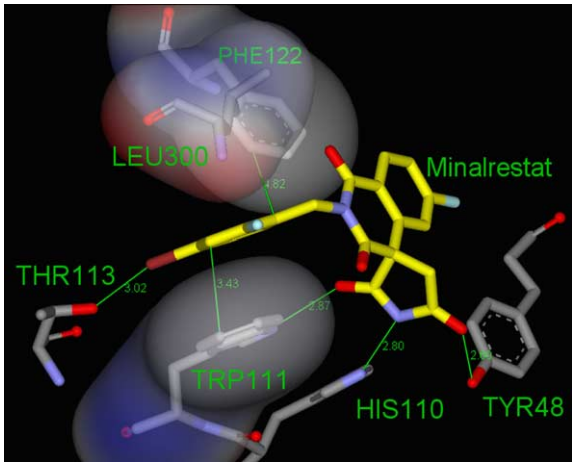

Figure 2. Examples of contacts (green lines with corresponding distances shown in Å) for Minalrestat with ALR2. These include polar contacts, corresponding to hydrogen bonds or electrostatic interactions, or hydrophobic contacts (surfaces) corresponding to zones of excluded waters. Note that the polar contacts, measured in the mass spectrometry experiments, involves residues 48 and 110–113, which are apart in the sequence.

2. Results and discussion

2.1. Gas-phase stability study by mass spectrometry

The gas-phase stability of the ALR2–inhibitor interaction was determined by CID-MS experiments (see Experimental section) for the enzyme complexes formed between ALR2 and the compounds Minalrestat, Fidarestat (2*S*4*S*) and the 2*R*4*S*-isomer (Scheme 2). It was not possible to measure the gas-phase stability of the 2*S*4*R* and 2*R*4*R*-isomers because of the presence of multiadducts, an indication of nonspecific binding. Additionally, the interaction of ALR2 with the inhibitors Statil and Sorbinil was determined in order to characterise the binding interaction of the two classes of inhibitors (Scheme 1). A comparison of the crystal structures of ALR2 in complex with Minalrestat[16] and Statil[21] has shown that these two inhibitors bind to the enzyme in a similar manner, suggesting that the orientations of the cyclic imide and carboxylic acid inhibitors in the active site of ALR2 are dictated by both the hydrophobic ring system and the polar head groups of the inhibitors. Sorbinil, a cyclic imide inhibitor that lacks the carbamoyl group of Fidarestat (Scheme 1), is 102-fold less potent than Fidarestat and makes fewer interactions with residues from the C-terminal loop. The VC_{50} values determined for the inhibitors based on the gas-phase stabilities of their complexes are listed in Table 1.

An approximate calculation of the electrostatic interactions between the active site residues Tyr48, His110 and Trp111 and the polar heads of the inhibitors in the

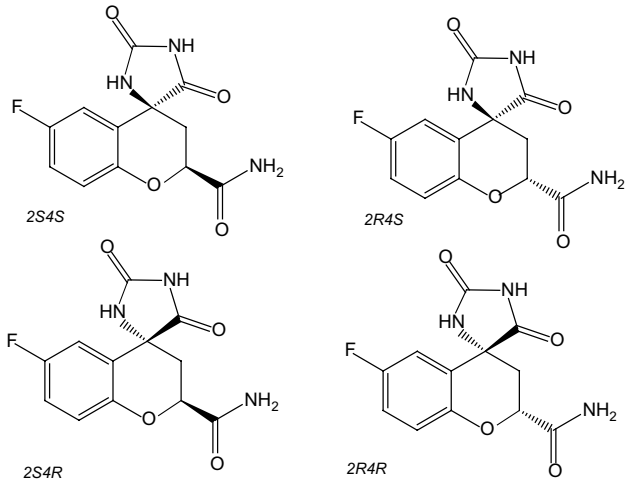

Scheme 2.

Table 1. Comparison of ALR2 inhibitor binding constants

Inhibitor	VC_{50} (V)	IC_{50}[a] (nM)	ΔH[b] (kcal/mol)
Fidarestat (2*S*4*S*)	56	9	−41
Statil	50.0	57	−31
Minalrestat	49.0	73	−27
Sorbinil	35.5	918	−19
2*R*4*S*	59	570	
2*S*4*R*		11,000	
2*R*4*R*		40,000	

[a] The IC_{50} values were reported by Hohman et al.,[26] Oka et al.[17] and Yamaguchi et al.[27]

[b] Intermolecular binding enthalpies (kcal/mol) between the active site residues Tyr48, His110 and Trp111 of human ALR2 and the bound inhibitors Fidarestat, Minalrestat, Sorbinil and Statil in the reported crystal structures. The corresponding gas-phase stabilities experimentally measured by mass spectrometry (VC_{50}) and the binding energies measured in solution (IC_{50} values) are listed. Due to non-specific binding between ALR2 and the 2*S*4*R* and 2*R*4*R*-isomers, the VC_{50} values for these compounds were not calculated.

reported crystal structures was obtained from molecular modelling. A correlation can be seen in Table 1 between the electrostatic component of the binding energy (ΔH), the gas-phase stability evaluated by the VC_{50} and the in vitro potency of the inhibitor (IC_{50}). The VC_{50} values range from 35.5 to 59 V with calculated binding energies ranging from −19 to −41 kcal/mol and IC_{50} values ranging from 9 to 40,000 nM. The similarity in the VC_{50} values displayed by Fidarestat and the 2*R*4*S*-isomer suggests that their complexes are equally stable in the gas phase. This would be expected given that the VC_{50} values mostly reflect the conserved electrostatic interactions between the cyclic imide substituents of the two compounds and the active site residues and do not reflect the favoured hydrophobic interactions between Fidarestat and the C-terminal residues, since these latter interactions do not exist in vacuum. The small difference in VC_{50} values for the two compounds (3 V) is likely a result of the relaxed C-terminal residues in the gas phase allowing a more favourable interaction between the cyclic imide substituent of the 2*R*4*S*-isomer and the active site residues. The correlation between the VC_{50} and IC_{50} values for the compounds suggests that the electrostatic interactions between the polar heads of the inhibitors and the active site residues play a major role in the stability of the enzyme–inhibitor complex, both in the gas phase and in solution. The largest differences for the VC_{50} and IC_{50} values can be seen between Sorbinil and both Fidarestat and the 2*R*4*S*-isomer. In this case the crystal structures of the enzyme–inhibitor complexes suggest that the additional contact between the carbamoyl group of Fidarestat and the C-terminal loop is responsible both for the enhanced gas phase and in-solution stability of the enzyme–inhibitor complex. On the other hand the small difference in the VC_{50} and IC_{50} values between Statil and Minalrestat is consistent with the conserved contacts between these two inhibitors and the C-terminal loop. Furthermore, our results suggest that the difference in the type of the polar head of the inhibitor (carboxylic acid vs cyclic imide) does not prominently influence the gas phase and in-solution stabilities of the enzyme complexes.

Table 2. Protein interaction energies (kcal/mol) calculated between ALR2 residues and compounds **1**–**9**

Compound	Protein interaction energy (kcal/mol)
1	−99
2	−91
3	−77
4	−71
5	−68
6	−124
7	−97
8	−86
9	−74

2.2. Molecular modelling and design

Molecular dynamics calculations were carried out for nine compounds, based on the structures of Fidarestat (compound **5**) and Minalrestat (compound **9**), as described in the Experimental section. Of those based on Fidarestat, the most favoured is compound **1** (see Table 2). Replacement of the carbamoyl group of Fidarestat with a carboxylate functional group (compound **1**) enhanced the net binding energies of the complex by 46% (−99 kcal/mol), while replacement with a 4-hydroxyl phenyl group (compound **2**) and a nitro group (compound **3**) enhanced the bindings by 34% (−91 kcal/mol) and 13% (−77 kcal/mol), respectively. On the other hand, the replacement of the carbamoyl group with a Br (compound **4**) had no significant effect on the binding (−71 kcal/mol), which is likely due to the limited number of new contacts introduced between this atom and the C-terminal residues. Compounds **1**, **2**, **3** and **5** (Fidarestat) were found to hydrogen bond to the side chains of Tyr48 OH (2.5, 2.7, 3.0 and 2.6 Å), Trp111 NE1 (3.2, 3.2, 3.9 and 2.7 Å), His110 Nε2 (3.0, 2.9, 3.0 and 2.8 Å) and Leu300 N (3.3, 3.9, 3.1 and 2.9 Å). The chroman rings of compounds **1** and **5** π-stack against the side chain of Trp20 (4.7 and 4.6 Å). The enhanced binding of compound **1** (−99 kcal/mol) compared to Fidarestat (compound **5**, −68 kcal/mol) reflects a favoured negatively charged carboxylate group over a carbamoyl group for the interaction with residues from the C-terminal loop. Compound **2** displayed a new hydrogen bond with Leu301 N (3.0 Å) as well as π-stacking of the chroman ring against Trp219 resulting in an enhancement in the binding energies of the complex (−91 kcal/mol). Residues within van der Waals contacts (4.0 Å) with compounds **5** and **1** are shown in Figures 3 and 4, respectively.

From the calculations based on Minalrestat, the most favoured is compound **6** (see Table 2). Replacement of the fluorine atom of Minalrestat's bromo-fluorobenzyl group (compound **9**) with a carboxylate probe (compound **6**) enhanced the net binding energies of the complex by 68% (−124 kcal/mol). Additionally, replacement with amide and nitro groups (compounds **7** and **8**) resulted in an increase in the net binding energies of the complexes by 31% (−97 kcal/mol) and 16% (−86 kcal/mol), respectively, after taking into account the energy losses due to the displacement of water molecules in the active site of the enzyme by the com-

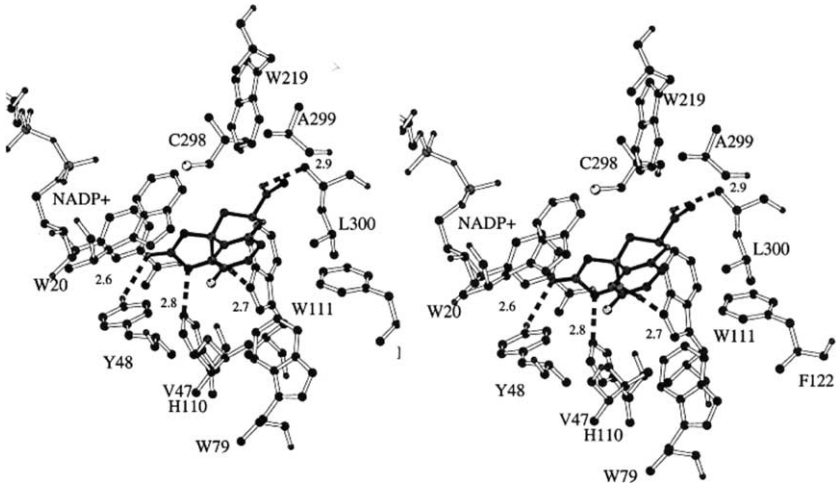

Figure 3. Stereoview of Fidarestat (compound **5**) bound into the active site of human ALR2. Residues within 4 Å of the inhibitor are shown. Hydrogen bonds (dashed lines) are drawn between the inhibitor and His110 Nε2 (2.8 Å), Tyr48 OH (2.6 Å), Trp111 (2.7 Å) and Leu300 N (2.9 Å). π-Stacking occurs between the inhibitor's chroman ring and Trp20 (4.6 Å).

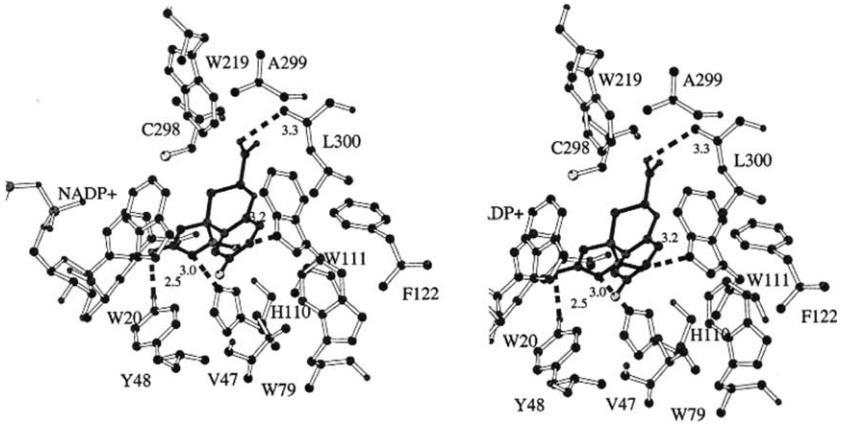

Figure 4. Stereoview of compound **1** bound into the active site of human ALR2 with residues within 4 Å shown. Hydrogen bonds between compound **1** and His110 Nε2 (3.0 Å), Tyr48 OH (2.5 Å), Trp111 NE1 (3.2 Å) and Leu300 N (3.3 Å) are shown as dashed lines. Similar to Fidarestat, there is π-stacking between the chroman ring of compound **1** and Trp20 (4.7 Å).

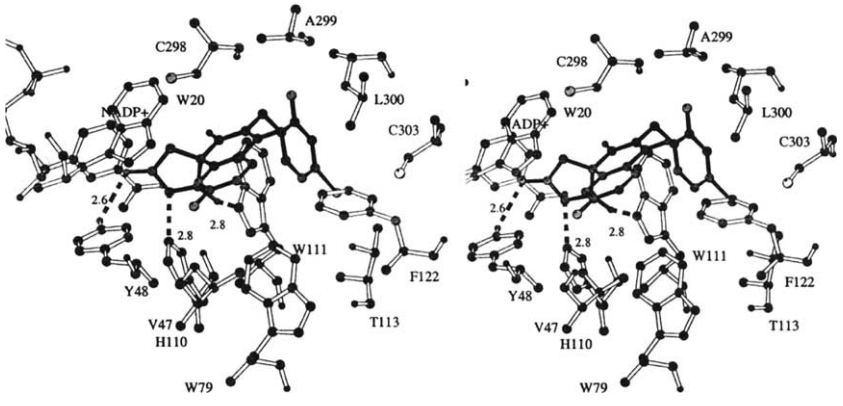

Figure 5. Stereoview of Minalrestat (compound **9**) bound into the active site of human ALR2 surrounded by residues within 4 Å. Hydrogen bonds occur between the inhibitor and His110 Nε2 (2.8 Å), Tyr48 OH (2.6 Å) and Trp111 NE1 (2.8 Å). The inhibitor's bromo-fluorobenzyl ring π-stacks against the side chain of Trp111 (3.5 Å) while the isoquinoline ring π-stacks against Trp20 (5.8 Å).

pounds. Residues present within van der Waals contacts of compounds **9** (Minalrestat) and **6** are shown in Figures 5 and 6, respectively. Both compounds are hydrogen bonded to the side chains of Tyr48 OH (3.2 and

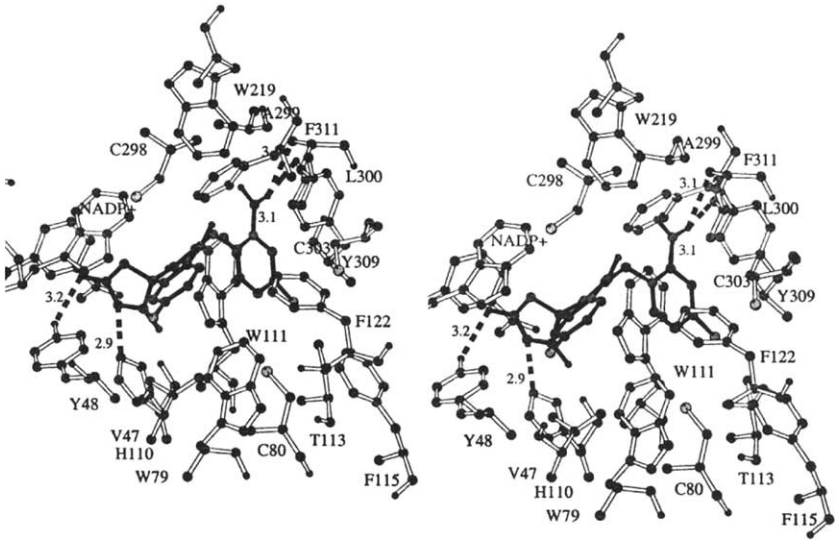

Figure 6. Stereoview of compound **6** (derivative of Minalrestat) modelled into the active site of ALR2. Hydrogen bonds are shown between compound **6** and His110 Nε2 (2.9 Å), Tyr48 OH (3.2 Å), Leu300 N (3.1 Å) and Tyr309 OH (3.1 Å). Similar to Minalrestat, compound **6** π-stacks against the side chains of Trp111 (3.8 Å) and Trp20 (4.6 Å). Figures were prepared using MOLSCRIPT.[28]

2.6 Å) and His110 Nε2 (2.9 and 2.8 Å). The benzene rings π-stack against the side chain of Trp111 (3.8 and 3.5 Å) and the isoquinoline rings π-stack against the side chain of Trp20 (4.6 and 5.8 Å). The enhanced binding of compound **6** (−124 kcal/mol) compared to Minalrestat (−74 kcal/mol) reflects the potential of forming additional contacts with residues from C-terminal loop, including a new hydrogen bond with Tyr309 OH (3.1 Å).

The binding enthalpies between the C-terminal residues and the designed compounds are listed in Table 3. A comparison of the binding enthalpies for compounds **1**, **2**, **3**, **4** and **5** indicated that the addition of a carboxylate (compound **1**), 4-hydroxyl phenyl (compound **2**), nitro group (compound **3**) and a bromide atom (compound **4**) to Fidarestat (compound **5**) enhanced the binding energies with the C-terminal residues by approximately 4, 4, 2 and 1 (i.e., no change) fold, respectively. Stronger interactions were found between compound **1** and Cys298 and Leu300 that resulted in a binding energy of −13 kcal/mol with these residues, enhancing the overall binding of the complex. Compound **2** also had stronger interactions with Leu300 and extra interactions with Ala299 and Ser302 resulting in a binding energy of −11 kcal/mol with these residues. Of the three compounds, compound **2** captured the most interactions with residues from the C-terminal loop but the overall binding of this complex was stronger than compound **5** and weaker than compound **1**. The modelling of the interactions between compounds **6**, **7**, **8** and **9** (Minalrestat) and the C-terminal loop, suggested that compound **6** resulted in a 4-fold enhancement in the binding energies and compound **7** showed a small improvement, while compound **8** showed weaker binding. Compound **7** showed enhanced binding with Leu300 and Tyr309, which explains the slightly higher energy of interaction (−11 kcal/mol) compared to compound **9** (−10 kcal/mol). Compound **8** had weaker interactions with Leu300 and Cys298, which decreased the energy of interactions slightly (−9 kcal/mol). Compounds **6** and **9** have similar interactions with the C-terminal residues but the interactions are much stronger in compound **6**, particularly with Ala299, Leu300 and Tyr309, increasing the overall binding energy with the C-terminal loop to −38 kcal/mol.

A comparison of the binding energies of all complexes suggested that the complex with compound **6** displays

Table 3. Comparison between binding constants of compounds **1**–**9**[a]

Residues	Δ*H* (kcal/mol)								
	1	**2**	**3**	**4**	**5**	**6**	**7**	**8**	**9**
Cys298	−5	−2	−2	−2	−3	−7	−1	−2	−3
Ala299		−2	−1			−8	−1	−1	
Leu300	−8	−5	−2	−1		−10	−5	−1	−4
Leu301			−1						
Ser302		−2				−1			
Cys303								−2	−1
Tyr309						−11	−2	−2	−1
Phe311						−1	−2	−1	−1

[a] Intermolecular binding enthalpies (kcal/mol) calculated between the C-terminal residues Cys298, Ala299, Leu300, Leu301, Ser302, Cys303, Tyr309 and Phe311 lining the 'specificity' pocket of ALR2 and the bound compounds **1**–**9**. Only values $\leqslant -1$ kcal/mol are shown.

the maximum binding energies (−124 kcal/mol) as well as capturing the maximum interactions with the residues from the C-terminal loop (−38 kcal/mol). Of particular interest are the unsuccessful attempts to model the above compound into the active site of ALR1 due to steric hindrance between the compound and nonconserved residues from the C-terminal loop, and therefore this compound may show more selectivity towards ALR2 over ALR1.

3. Conclusion

The correlation (Table 1) between the electrostatic component of the binding energy (ΔH), gas-phase stability (VC_{50}) and inhibitor potency (IC_{50}) suggests that the interactions between the polar heads of the inhibitors and the active site residues play a major role in the overall stability of the enzyme–inhibitor complexes. The additional interaction between the carbamoyl group of Fidarestat and the C-terminal loop of ALR2 resulted in the enhancement of both the gas-phase and in-solution stability of this complex compared to the ALR2–Sorbinil complex. In the case of the complexes of ALR2 with Minalrestat and Statil, the small difference in the VC_{50} and IC_{50} values reflects the conserved interactions between the C-terminal loop in ALR2 and these two inhibitors. Our molecular modelling and design studies suggest that the replacement of both Minalrestat's fluorine atom and Fidarestat's carbamoyl group with a carboxylate functional group (compounds **1** and **6**) may enhance the net binding energies of the enzyme–inhibitor complexes. These newly designed compounds may capture the maximum interactions with nonconserved residues from the C-terminal loop of ALR2, providing the basis for a structure-based design approach of inhibitors that are more specific to ALR2 than ALR1 and decreasing the potential for the development of undesirable side effects.

4. Experimental

4.1. Expression and purification of ALR2

The open reading frame of the human ALR2 gene (Accession Gene Bank/EMBL Data Bank Number J05017) was amplified by PCR from cDNA[22] and cloned into T7 RNA polymerase-based vector pET15b (Novagen). Expression of hexahistidine tagged protein in *Escherichia coli* strain BL21(DE3) (Novagen) was induced by IPTG (Euromedex) during a 3-h period at 37 °C. The pellet from a 4-L culture was disrupted by sonication and centrifuged. The supernatant was loaded onto a Talon metal-affinity column (Clonetech). After thrombin cleavage of the hexahistidine extension, the detagged protein was loaded onto a DEAE Sephadex A-50 column (Pharmacia) and eluted with a NaCl gradient.[22]

4.2. Sample preparation for mass spectrometry

ALR2 was further desalted by five dilution stages (5 × 60 min) in 10 mM ammonium acetate (pH 7.0) by using Centricon PM 10 micro-concentrators (Millipore). The final enzymatic concentration was spectrometrically measured (UV, 280 nm). The proteins were stored at 4 °C in 10 mM ammonium acetate and used within a week after the end of their purification. The inhibitors were prepared as highly concentrated solutions (5 mM) in ethanol. These solutions were then diluted to 100 μM in 10 mM ammonium acetate (pH 7.0). The coenzyme $NADP^+$ was purchased as a salt free powder from Boehringer–Mannheim and dissolved to 1 mM in 10 mM ammonium acetate (pH 7.0). The enzyme–inhibitor complexes were prepared by incubating the enzyme diluted to 10 μM in 10 mM ammonium acetate with 1 equiv of $NADP^+$ and 1 equiv of inhibitor. After a short incubation time at room temperature, the samples were continuously infused into the ESI ion source at a flow rate of 5 μL/min.

4.3. Mass spectrometric measurements

An electrospray-time-of-flight mass spectrometer (ESI-TOF) equipped with a *Z*-ion source (LCT from Micromass) was used to perform the measurements. Electrospray ionisation (ESI) conditions were optimised in order to keep the noncovalent specific interactions during ion desorption in the gas phase, while ensuring a good desolvation of the sprayed droplets. Details of the optimisation procedure have been given elsewhere.[18] Briefly, two parameters are concerned: the accelerating voltage of ions *Vc* and the pressure in the cone-to-skimmer interfacial region of the mass spectrometer ($P_{\text{interface}}$). *Vc* defines the electrostatic field in the cone-to-skimmer region. Increasing *Vc* increases the internal energy transferred to ions through collisions with residual gaseous molecules, which provokes disruption of the weaker interactions. Gas-phase stabilities of noncovalent complexes can thus be measured by their resistance to energetic collisions as a function of the accelerating voltage *Vc*. $P_{\text{interface}}$ is involved in the mean free path of ions and thus in the kinetic energy acquired between two collisions: the higher $P_{\text{interface}}$, the lower the kinetic energy of the ions and the milder the collisions. $P_{\text{interface}}$ as well as *Vc* intervene in the internal energy that is transferred to the ions upon collision in the interface. They need to be tuned in a compromised manner so to keep a nice quality signal while preserving the weak interactions of interest. Noncovalent ALR2–$NADP^+$–inhibitor complexes were submitted to CID (collision induced dissociation) experiments in order to evaluate their relative gas-phase stabilities. In these measurements, $P_{\text{interface}}$ was carefully controlled and kept constant at 5 mbar. First, *Vc* was tuned in order to observe the intact noncovalent complexes; then it was increased stepwise in order to produce the disruption of ALR2–inhibitor interaction in the gas phase. Progressive dissociation of the noncovalent protein–ligand complexes were monitored by the appearance of ions corresponding to the unbound species in the mass spectrum. An

example is given in Figure 7. The VC_{50} values (accelerated voltage of ions needed to achieve 50% of dissociation of a noncovalent complex in the gas phase) measured for the ARIs Fidarestat, 2*R*4*S*-isomer, Minalrestat, Sorbinil and Statil are listed in Table 1. These values are deduced from dissociation curves as the one shown in Figure 7.

4.4. Molecular modelling calculations

The atomic resolution refinement of the ALR2 holoenzyme complexes with the cyclic imide inhibitors Fidarestat and Minalrestat allowed the positioning of

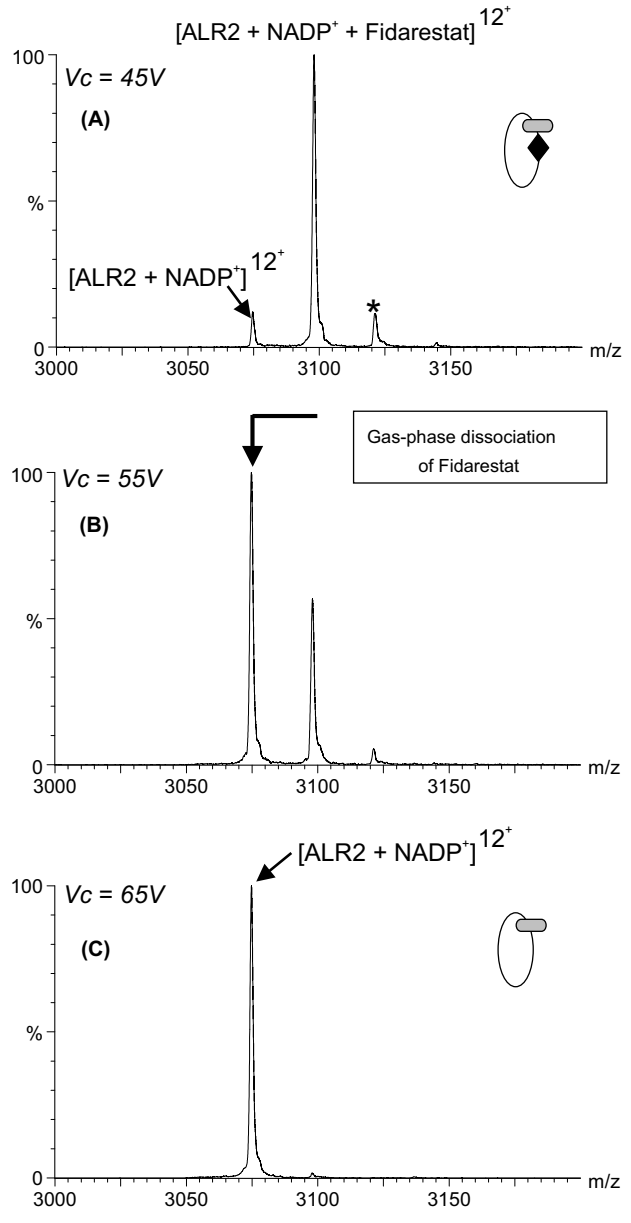

Figure 7. Gas-phase stability study of ALR2–Fidarestat complex. ESIMS spectra were recorded for increasing values of *Vc*: $Vc = 45$ V (A); $Vc = 55$ V (B); $Vc = 65$ V (C). The enzyme–inhibitor complex gradually dissociates when *Vc* increases. The peak labelled with a star corresponds to a second adduct of ligand.

hydrogen atoms and accurate determination of bond lengths of the inhibitors, coenzyme $NADP^+$ and active site residue His110.[16] The imidazole ring of His110 was protonated at the Nε2 atom position and formed a hydrogen bond with the negatively charged 1′-position nitrogen atom of the cyclic imide rings of the inhibitors. Note that the ultra-high resolution structures of ALR2 including crystallographically determined protonation states of cyclic imide inhibitors were crucial for the molecular modelling and design studies.

The program GRID (version 18)[23] was used to search the active site of ALR2 for the most suitable or favourable positions of a variety of probes. A total of 24 probes were tested, which included the following groups: methyl, aromatic carbon, amino, amido and heterocyclic nitrogens, halogens, sulfur, carbonyl, ether and hydroxy oxygens, carboxy group, water, phosphate and other ions. Each probe was analysed independently using the InsightII 2.1 package (Biosym Technologies Inc., San Diego, CA, USA). Calculations were performed on a cube (35 Å per side) centred on the active site, with a grid spacing of 0.5 Å. The interaction energy between the probe and every atom within the protein structure was evaluated at each grid point. A dielectric constant of 80 was used to simulate a bulk aqueous phase, while areas as determined by GRID to be excluded from solvent were assigned a dielectric constant of 4 (i.e., the interior of the protein). The accompanying program GRIN was used to automatically assign atom types and charges for the protein, using the standard parameter file provided with GRID. The output was converted (using GINS supplied with GRID) into a form suitable for input to the Biosym utility contour, and contour maps were built up in minimum steps of 0.5 kcal/mol. The contour map detailed a number of energy levels. Negative energy levels delineate regions at which ligand binding is particularly favoured while positive energy levels define the surface of the target. The contour map was then superimposed on the active site of ALR2 using InsightII. Superposition of the inhibitors Fidarestat and Minalrestat on the active site provided information on the predicted position of the probe with respect to the inhibitor. Table 4 summarises the GRID analysis results for the probes with the most significant energy levels in the vicinity of the C-terminal region of ALR2. There were seven favoured probes suggested by the GRID program, of which the phosphate group was the most favoured and the fluorine atom the least favoured. These probes were considered in the design and

Table 4. GRID analysis results showing the contour energy levels (kcal) within the active site of human ALR2 for the best seven probes

Probe	Max. energy (kcal)
Phosphate	−10
Bromine	−7
Carboxylate	−6
Amide	−6
Phenyl hydroxyl	−6
Nitro	−5
Fluorine	−4

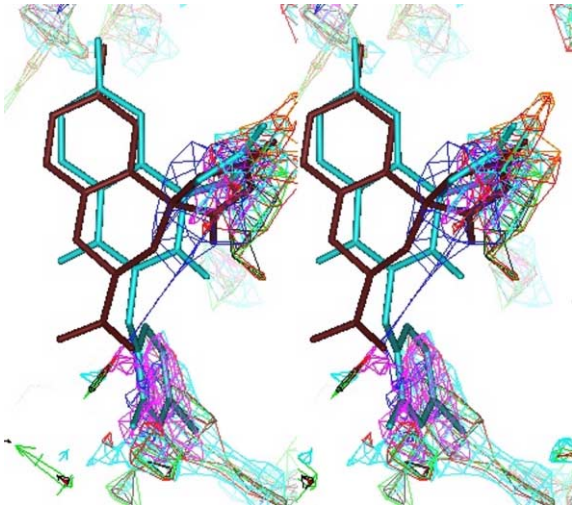

Figure 8. GRID results showing contours of interaction energies between the active site of human ALR2 and phosphate (blue), phenyl hydroxyl (green), carboxylate (red), amide (black), bromine (pink), nitro (cyan) and fluorine (orange) probes with the superimposed inhibitors Minalrestat (cyan) and Fidarestat (red). The figure was prepared using InsightII (Biosym Technologies, San Diego, CA).

modelling of new potential inhibitors of ALR2. The predicted regions of interactions between the active site of human ALR2 and the probes are shown in Figure 8.

Compounds **1**–**5** and **6**–**9** were designed based on the structures of Fidarestat and Minalrestat, respectively, to include the functional groups shown above (Scheme 3), so that each probe would be placed in its corresponding favoured region of interaction within the C-terminus, as suggested by the GRID analysis results. Additional compounds including different functional groups were also considered but were found too bulky to fit into the pocket due to steric hindrance with residues lining the active site.

The designed compounds were docked into the active site of ALR2 based on the orientation of Fidarestat and Minalrestat in the crystal structures.[16] Energy minimisation and molecular dynamics calculations were carried out using the Discover 2.7 package (Biosym Technologies, San Diego, CA, USA), on an O2 (R12000) workstation (Silicon Graphics, Mountain View, CA, USA) following established procedures found to be effective in examining conformational space with a protein–ligand complex.[24,25] Waters present in the active site that coincided with the docked compounds were removed. Arginine, lysine, aspartate and glutamate amino acids were charged while the histidines were uncharged, with hydrogen atoms fixed at the Nε2 atom. The constant valence force field incorporating the simple harmonic function for bond stretching and excluding all nondiagonal terms was used (cut-off distance of 31 Å). Calculations were done using the algorithms steepest descents and conjugate gradients (down to a maximum atomic root-mean-square derivative of 10.0 and 0.01 kcal/Å, respectively). In order to simulate an aqueous environment and to prevent residues on the surface from deviating significantly, the active site of ALR2 was solvated by a 15 Å layer of water molecules using the SOAK option of InsightII. Molecular dynamics were then performed using leapfrog algorithms in Discover. Dynamics were equilibrated for 2 ps with time steps of 1 fs and then continued for 4 ps with time steps of 2 fs at 350 K. The resulting structures were extracted and energy minimised. The structures were visualised by using InsightII and the interactions between the compounds and the ALR2 active site residues were analysed. The binding energies were calculated by Discover taking into account energy losses due to water displacement by the compounds in the active site.

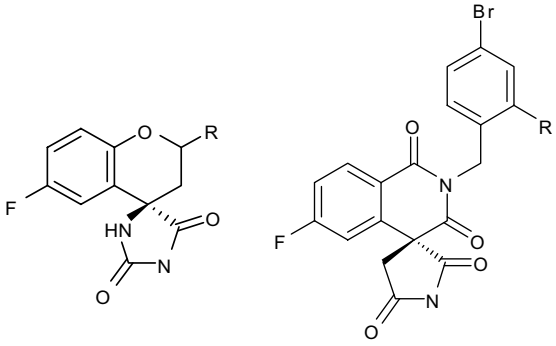

1. (R=COO^-)
2. (R=4-hydroxyl phenyl)
3. (R = CH_2ONO)
4. (R=Br)
5. (R = amide/Fidarestat)

6. (R=COO^-)
7. (R = amide)
8. (R= CH_2ONO)
9. (R=F/munalrestat)

Scheme 3. Designed compounds based on the structures of Fidarestat (left) and Minalrestat (right).

Acknowledgements

This work was supported in part by the Australian Research Council to OE-K. G.C. gratefully acknowledges the CNRS and Aventis for financial support. A.P. gratefully acknowledges the CNRS, the Institut National de la Santé et de la Recherché Médicale and the Hôpital Universitaire de Strasbourg (H.U.S.) for support.

References and notes

1. Kintoshita, J. H.; Nishimura, C. *Diabetes Metab. Res.* **1988**, *4*, 323.
2. Dunlop, M. *Kidney Int. Suppl.* **2000**, *77*, S3.
3. Costantino, L.; Rastelli, G.; Vianello, P.; Cignarella, G.; Barlocco, D. *Med. Res. Rev.* **1999**, *19*, 3.
4. Yabe-Nishimura, C. *Pharmacol. Rev.* **1998**, *50*, 21.
5. Costantino, L.; Rastelli, G.; Gamberini, M. C.; Barlocco, D. *Exp. Opin. Ther. Patents* **2000**, *10*, 1245.
6. Jez, J. M.; Bennett, M. J.; Schlegel, B. P.; Lewis, M.; Penning, T. M. *Biochem. J.* **1997**, *326*, 625.
7. Warren, J. C.; Murdock, G. L.; Ma, Y.; Goodman, S. R.; Zimmer, W. E. *Biochemistry* **1993**, *32*, 1401.
8. El-Kabbani, O.; Wilson, D.; Petrash, J. M.; Quiocho, F. A. *Mol. Vis.* **1998**, *4*, 19.
9. El-Kabbani, O.; Old, S. E.; Ginell, S. L.; Carper, D. A. *Mol. Vis.* **1999**, *5*, 20.

10. Urzhumtsev, A.; Tête-Favier, F.; Mitschler, A.; Barbanton, J.; Barth, P.; Uzhumtseva, J. F.; Biellmann, A. D.; Podjarny, A.; Moras, D. A. *Structure* **1997**, *5*, 601.
11. Kaul, C. L.; Ramarao, P. *Methods Find. Exp. Clin. Pharmacol.* **2001**, *23*, 465.
12. Oates, P. J.; Mylari, B. L. *Exp. Opin. Invest. Drugs* **1999**, *8*, 1.
13. Pfeifer, M. A.; Schumer, M. P.; Gelber, D. A. *Diabetes* **1997**, *46*, S82.
14. Miyamoto, S. *Expert. Opin. Ther. Patents* **2002**, *12*, 621.
15. Rastelli, G.; Ferrari, A. M.; Costantino, L.; Gamverini, M. C. *Bioorg. Med. Chem.* **2002**, *10*, 1437.
16. El-Kabbani, O.; Darmanin, C.; Schneider, T. R.; Hazemann, I.; Ruiz, F.; Oka, M.; Joachimiak, A.; Schulze-Briese, C.; Tomizaki, T.; Mitschler, A.; Podjarny, A. *Proteins* **2004**, *55*, 805.
17. Oka, M.; Matsumoto, Y.; Sugiyama, S.; Tsuruta, N.; Matsushima, M. *J. Med. Chem.* **2000**, *43*, 2483.
18. Rogniaux, H.; Van Dorsselaer, A.; Barth, P.; Biellmann, J.-F.; Bardanton, J.; Van Zandt, M.; Chevrier, B.; Howard, E.; Mitschler, A.; Potier, N.; Urzhmtseva, L.; Moras, D.; Podjarny, A. *J. Am. Soc. Mass Spectrom.* **1999**, *10*, 635.
19. El-Kabbani, O.; Rogniaux, H.; Barth, P.; Chung, R.; Fletcher, E.; Dorsselaer, A.; Podjarny, A. *Proteins* **2000**, *41*, 407.
20. Loo, J. A. *Mass Spectrom. Rev.* **1997**, *16*, 1.
21. El-Kabbani, O.; Ramsland, P.; Darmanin, C.; Chung, R.; Podjarny, A. *Proteins* **2003**, *50*, 230.
22. Chung, S.; La Mendola, J. *J. Biol. Chem.* **1989**, *264*, 4775.
23. Goodford, P. J. *J. Med. Chem.* **1985**, *28*, 849.
24. Darmanin, C.; El-Kabbani, O. *Bioorg. Med. Chem. Lett.* **2001**, *11*, 3133.
25. Darmanin, C.; El-Kabbani, O. *Bioorg. Med. Chem. Lett.* **2000**, *10*, 1101.
26. Hohman, T. C.; El-Kabbani, O.; Malamas, M. S.; Lai, K.; Putilina, T.; McGowan, M. H.; Wane, Y.-Q.; Carper, D. A. *Eur. J. Biochem.* **1998**, *256*, 310.
27. Yamaguchi, T.; Miura, K.; Usui, T.; Unno, R.; Matsumoto, Y.; Fukushima, M.; Mizuno, K.; Kondo, Y.; Baba, Y.; Kurono, M. *Arzneim.-Forsch./Drug Res.* **1994**, *44*, 348.
28. Kraulis, P. J. *J. Appl. Cryst.* **1991**, *24*, 946.